PROCEEDINGS OF SCIENCE

Status and recent results from the Radio Neutrino Observatory in Greenland (RNO-G)

S. Hallmann[a,*] **for the RNO-G Collaboration**

(a complete list of authors can be found at the end of the proceedings)

[a] *Deutsches Elektronen-Synchrotron (DESY), Platanenallee 6, 15738 Zeuthen, Germany*

E-mail: steffen.hallmann@desy.de

The Radio Neutrino Observatory in Greenland (RNO-G) is an in-ice radio detector for the detection of ultra-high energy neutrinos beyond ~10 PeV. The array is under construction and will consist of 35 stations, with the potential to make the first detection of a neutrino-induced particle shower via the Askaryan emission. Stations operate autonomously and consist of both deep antennas deployed down to -100 m in the ice, and high-gain log-periodic dipole antennas buried near the surface.

In total, seven RNO-G stations were installed during the 2021 and 2022 field seasons and are collecting data since. Here, we present the current status and performance of the experiment. We present results from first analyses using the deep and shallow components of the instrument.

The 38th International Cosmic Ray Conference (ICRC2023)
26 July – 3 August, 2023
Nagoya, Japan

*Speaker

PoS(ICRC2023)1043

1. RNO-G station design

The Radio Neutrino Observatory in Greenland (RNO-G) [1] is under construction at Summit Camp, on the apex of Greenland's ~3000 m thick ice sheet. With 35 stations spaced by 1.25 km it will reach an effective area with the potential to detect the first neutrino-induced in-ice particle showers via the Askaryan emission at ultra-high energies (UHE), beyond ~10 PeV.

Building on the experience gained with the preceding smaller scale radio arrays – in particular ARIANNA, ARA, and ANITA [2] – the RNO-G station layout depicted in Fig. 1 (left) is a combination of nine log-periodic dipole antennas (LPDAs) buried in shallow trenches and 15 deep antennas sensitive to the vertical (Vpol; 11 channels) or horizontal (Hpol; 4 channels) signal components. The deep antennas are distributed over three 11 inch wide holes that are drilled down to -100 m using the BigRAID, a custom auger drill by the British Antarctic Survey [3]. The arrangement of the deep antennas allows for energy and direction reconstruction of the neutrino-induced shower. Their depth provides a large neutrino-effective area. To this end, four of the Vpol antennas are closely packed at -100 m and designed to act as a phased array trigger to lower the detection threshold of the instrument. The Hpol antennas improve the direction resolution when they pick up a signal strong enough to reconstruct the polarization. However, their design is challenging due to the limited diameter of the hole. The RNO-G Hpols are quad slot antennas; their design and performance are presented in detail in Ref. [4]. While LPDAs provide the possibility for an additional verification of a detected neutrino signal, they are particularly valuable to identify and study (or veto) cosmic ray air showers and other (predominantly anthropogenic) noise sources originating from the surface. The installation is shown in Fig. 1 (right).

An overview of the construction status of the detector is given in Sec. 2. First analysis results

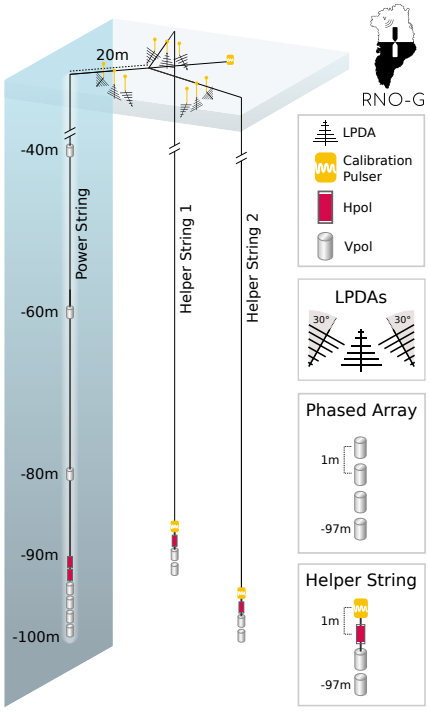

Figure 1: Layout of the hybrid RNO-G station *(left)* with LPDA antennas deployed in shallow trenches, and Vpol and Hpol antennas installed in the deep boreholes. The deployment process for the shallow *(top-left)* and deep *(top-right)* components, respectively, is illustrated above.

are presented in Sec. 3. Finally, in Sec. 4, the neutrino sensitivity of the full detector, in particular in the multi-messenger context, and an outlook to possible enhancements are given.

2. Construction status and 2023 field season

Currently, seven stations are installed and record data. The first three stations were installed in 2021. Four more stations were added in 2022 with an upgraded power system, improved shielding against electromagnetic interference, and additional filters. These improvements successfully suppress self-induced noise from battery charging during daytime and data transmission to Summit Camp, respectively, that was observed in the first stations. Solar panels provide autonomous power for continuous full station operation for about half of the year, with the option to extend operation to ~66% up-time by running in low-power mode without the phased array trigger and/or pausing the data acquisition for parts of the day when the Sun is below the horizon [1]. Prototype wind turbines were set up and tested in 2021 at two stations to work towards the possibility of year-round data-taking. In 2022, data-taking was stopped for the winter around 01 October and resumed around 24 April 2023 in most stations, corresponding to a 56% annual fraction spent in winter mode.

The 2023 field season was used for station maintenance, positioning via GPS and ground-penetrating radar, and a calibration campaign. At the moment, the index of refraction in the firn is the largest unknown in the antenna position calibration efforts. Position calibration relies mainly on two in-situ pulsers at 95 m depth and one near-surface pulser. This is complemented by calibration pulsing from fixed GPS positions during field seasons and other intermittent background sources. Ref. [5] elaborates on the ice modelling and antenna position calibration in detail. A recently bought melting probe depicted in Fig. 2 was tested in the field. Without continuous supervision, the probe can melt 13 cm diameter holes to 30 m depth. With these holes it is possible to install the near-surface pulser deeper into the firn, which allows for better calibration in the firn ice. A thorough description of the detector calibration efforts can be found in Ref. [6]. The installation of up to ten additional stations will continue in 2024. The construction of the station hardware and a firmware upgrade for the BigRAID drill are already in preparation.

3. RNO-G station performance and first analysis results

The trigger rates for two stations are shown in Fig. 3. The stations currently operate with several active triggers: a fraction of the signal from all channels is split off to a triggering diode on which threshold coincidences can be formed. This diode trigger path is currently used for two surface triggers requiring 2-fold coincidences on the upward- or downward-facing LPDAs, respectively. The signal of the four bottom Vpols of the “power string" is split off to a separate board with low power consumption designed to form the phased-array trigger. At the moment, data on this trigger board is recorded on a two-fold threshold coincidence as well. In addition, minimum-bias triggers are taken with a rate of 0.1 Hz. A detailed description of the RNO-G hardware can be found in Ref. [7].

Compared to the 2021 station hardware, the trigger rates in Fig. 3 are stable during the day for the revised design, with no sign of remaining strong self-induced noise sources. In particular the deep trigger does not show obvious dependency on daytime and the bulk of waveforms is compatible

Figure 2: Melting probe in operation during the 2023 RNO-G field season.

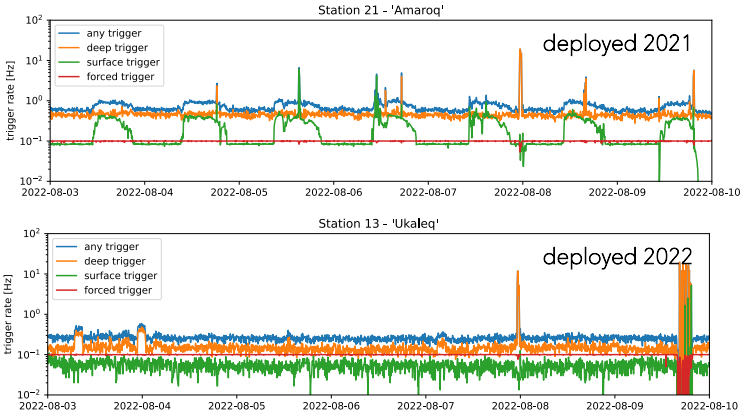

Figure 3: Trigger rates for one week of data-taking for a station deployed in 2021, and a station deployed in 2022 with upgraded power system and added filters. For the new station, a series of calibration runs are visible on 2022-08-09. A weather balloon is visible in both stations on 2022-08-08. The 2021 station is closest to Summit Camp. Figure taken from Ref. [8].

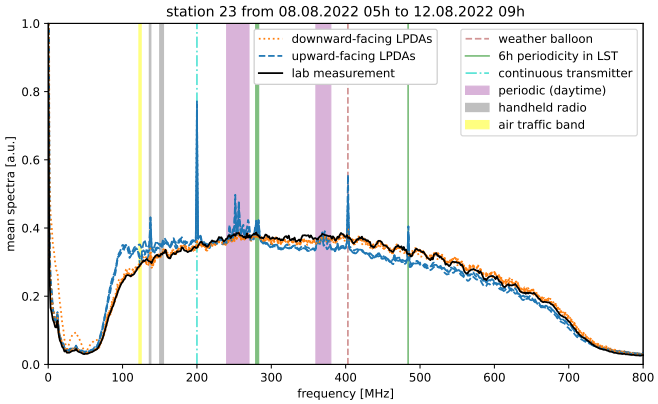

Figure 4: Average frequency spectra observed in the upward- and downward-facing LPDAs. A lab measurement of average noise spectra of the DAQ system alone is added for comparison. The spectra are normalised with respect to each other in the 500–650 MHz region. Known narrowband and broadband backgrounds are indicated in the legend.

with thermal noise. This suggests that anthropogenic backgrounds at the site are mostly seen by the surface LPDAs but do not constitute a dominant persistent noise source in the deep antennas.

Fig. 4 shows the average frequency spectra observed in the upward- and downward-facing surface LPDAs. The agreement of the spectrum seen by the downward-facing LPDAs with a measurement of the DAQ system noise shows that they see predominantly thermal noise only. In contrast, several narrow and broadband backgrounds originating from the surface or above are visible in the upward-facing LPDAs.

3.1 Observed classes of anthropogenic and (near-)station backgrounds

The narrow- and broadband backgrounds seen in the RNO-G stations are summarized in Fig. 4. A strong narrowband background at 403 MHz is seen twice a day when weather balloons are launched near Summit Camp and pass over the array. Additional narrowband lines from air traffic, handheld radio and satellite communication are visible intermittently. A background from a continuous transmitter at 200 MHz is constantly visible in several stations. Its origin is currently still

under investigation. Impulsive and broadband backgrounds occur when there is activity on Summit Camp and are more prominent during daytime. In particular, snowmobiles and the operation of heavy machinery at Summit Camp or the skiway can produce impulsive events when they pass close to a station. In addition, wind speeds above ∼10 m/s are known to generate wind-induced backgrounds, suspected to occur when metal surfaces on the snow get charged and subsequently discharge. This so-called triboelectric effect is observed also in RNO-G [9]. The electronics of the wind turbines were observed to also generate noise initially, which could be mitigated in the 2023 field season. As opposed to neutrino events, all of the described backgrounds are generated on top of or above the snow surface.

Machine-learning-based analyses are being developed to find features and noise classes observed in data. Variational autoencoders are used for this task that consist of an encoding part, a bottleneck layer and a decoding part of the network. The low dimensionality of the bottleneck will then learn to encode the most relevant features in the data during training.

One method, presented in Ref. [10], uses clustering algorithms on the bottleneck to identify frequent classes of events. The analysis is able to discriminate thermal noise, continuous wave backgrounds and impulsive events. Interestingly, the clustering shows an intriguing sub-structure on events attributed to wind. Another method, presented in Ref. [11], uses the mean average error (MAE) between the original and the reconstructed image sent through the trained network to identify outliers in the data. This method shows an increase in the MAE value in the presence of transient backgrounds, such as the passage of snowmobiles near a station or the occurrence of solar flares. The response of this method to a possible neutrino signal in the data is still to be studied.

3.2 Non-anthropogenic signals observed in RNO-G

In addition to the various anthropogenic backgrounds described and identified above, there are three notable sources of radio emission of extraterrestrial origin which have been studied in RNO-G data so far: The thermal emission by the Galaxy, flaring activity of the Sun, and radio signals induced by cosmic-ray air-showers.

The diffuse thermal emission by the Galaxy is dominant over the instrument noise below ∼ 120 MHz. The rise of the thermal noise towards lower frequencies in the upward-facing LPDAs is also visible in Fig. 4. Since the galaxy is spread over the sky, and with the central part of the galaxy below the horizon for RNO-G, the variation in the galactic noise temperature over the day seen in the antennas is relatively small. In the upward-facing LPDAs, a daily variation of the power in the low frequency band is observed as a function of local sidereal time. This is shown in Fig. 5. The daily trend is consistent with the expectation from simulations using the NuRadioReco [12] software framework. The absolute normalisation is dependent on the final voltage calibration and is still under investigation. Once the absolute normalisation is settled, this galaxy signal may be used as a standard candle for future station calibrations.

Compared to the Galaxy, the constant thermal emission from the Sun only has a small contribution, not surpassing 6% relative to the Galaxy below 200 MHz [13]. However, several solar flares occur in the frequency range and field of view relevant to RNO-G per week. In Fig. 6, the elevated trigger rate and the frequency spectra for one visible solar flare are shown. For comparison, a solar flare monitor for the HUMAIN observatory of the e-Callisto network [14, 15], pointed towards the

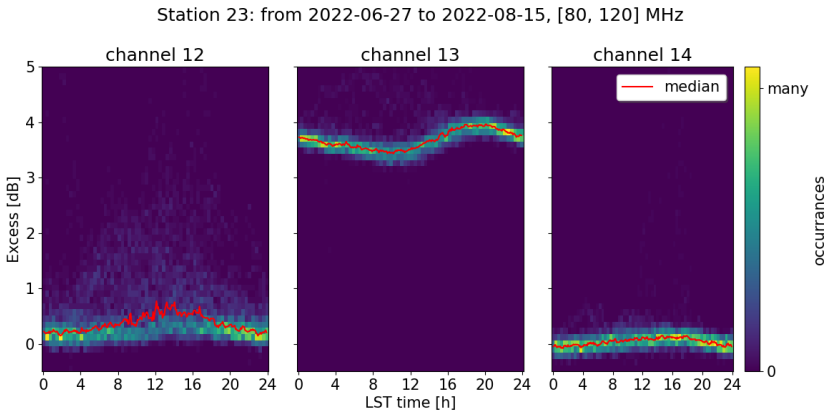

Figure 5: Variation of the power in the frequency spectrum integrated between 80 MHz and 120 MHz for recorded forced trigger data as a function of local sidereal time. The excess is calculated with respect to the hardware thermal noise frequency spectrum normalised to data in the high-frequency range (cf. black line in Fig. 4).

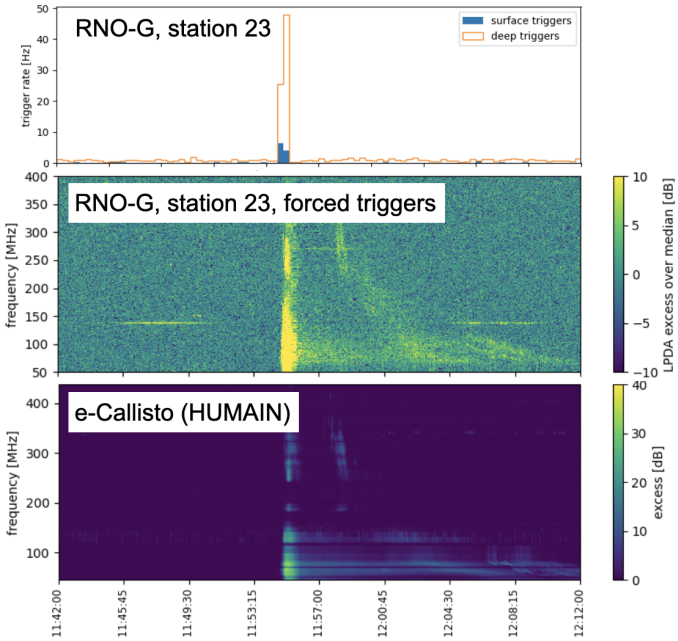

Figure 6: Trigger rates and excess in the upward-facing LPDA frequency spectrum for forced triggers observed in RNO-G during a solar flare on 09/29/2022. The frequency spectrum observed in the solar flare monitoring HUMAIN instrument as part of e-Callisto [14, 15] is shown for comparison.

Sun is added. While the latter instruments are more sensitive towards detecting solar flares, these events represent a background and calibration source for RNO-G.

RNO-G is expected to see several cosmic-ray air showers per day per station, with absolute numbers depending on the precise modelling of the surface trigger diode [16]. A correlation analysis is being developed which is able to cover the full parameter space of possible cosmic ray air shower signals using a small set of Gaussian pulse templates folded with the instrument response. The three upward-facing LPDA antennas are used to identify cosmic-rays since they have the highest sensitivity to in-air radio emission. The analysis has been run on a small sub-sample of the satellite-transferred data and identified first candidate events. The reconstructed signal arrival

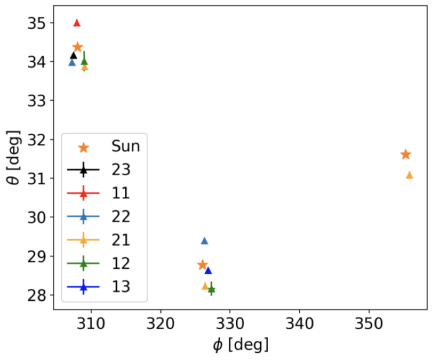

Figure 7: Reconstructed direction of events seen in the deep antennas of different RNO-G stations for three solar flares. A preliminary antenna position calibration was used for reconstruction.

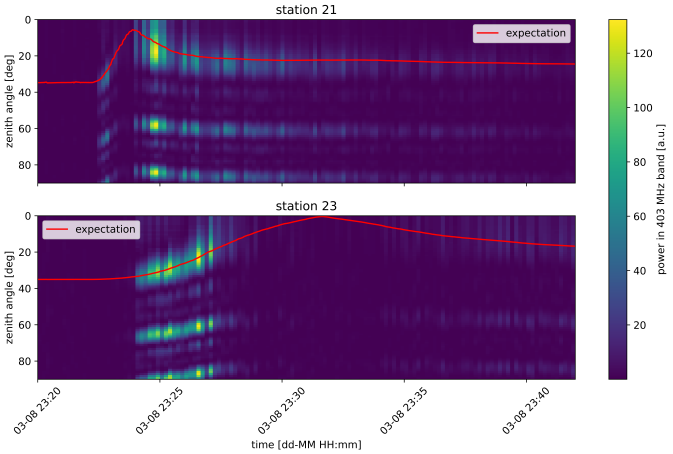

Figure 8: Weather balloon seen with the phased array. The color code shows the coherently summed power in the 403 MHz line (arbitrary units) after beamforming. Since the signal is periodic, side-maxima are observed.

direction and polarisation are consistent with a cosmic ray hypothesis. The method and results of the analysis are presented in Ref. [17].

3.3 Verification of the instrument pointing

Since all of the backgrounds shown above originate on top of the snow surface, accurate triangulation of a received signal is important to discriminate neutrino candidate signals from background. There is one additional background from UHE atmospheric muons generated in cosmic-ray air-showers that penetrate the ice and may produce in-ice particle showers along their track. The expected absolute rate strongly depends on the flux and hadronic interaction models, but is found to be <0.1 events per year of operation with the full 35-station RNO-G detector [18].

A reconstruction method using forward folding has been presented, that achieves a median direction resolution of 7° on simulations [19]. Waiting for the final antenna position calibration, a preliminary verification of the pointing is obtained by reconstructing the origin of the impulsive solar flare events occurring during bright flares. This is shown in Fig. 7 using data from solar flares. The phasing approach is verified by adding the received waveforms of the four phased array Vpols to form coherent beams towards all possible zenith angles. The power of the 403 MHz line emitted by the weather balloon is shown as a function of the zenith angles as a function of time. The agreement with the true expected arrival zenith is visible in Fig. 8.

4. RNO-G sensitivity and physics potential

RNO-G is the first production scale implementation of a radio array, which will be sensitive to confirm or reject a range of predicted realistic GZK and UHE astrophysical neutrino fluxes. During the upcoming years, RNO-G will not only be the detector with the largest neutrino-effective area in the UHE range, but also the only UHE neutrino observatory monitoring the northern hemisphere, with a field of view that coincides with the region where IceCube has its best sensitivity at neutrino

energies in the multi-TeV range. With the detection of the first neutrino sources by IceCube and the gravitational wave observatories online, RNO-G will play a unique role in the UHE neutrino and multi-messenger landscape in the upcoming years. RNO-G's sensitivity in the multi-messenger context is studied in more detail in Ref. [20]. In addition, further development is also ongoing towards improving the DAQ system to reach an even higher neutrino sensitivity. One possibility is to lower the trigger threshold for individual beams of the phased array trigger in case of an external alert falling into that beam's direction. This 'transient mode' would achieve up to a factor two improvement in instantaneous aperture [20]. It is also investigated if a machine-learning-based trigger can be deployed to the RNO-G data acquisition hardware. The possible enhancement in sensitivity is studied in Ref. [21] and has the potential to increase the trigger effective area by 70% at the threshold, and by 15% at the highest energies.

These possible future improvements, even if they may not be realised in RNO-G soon, are also relevant for the proposed larger radio array as part of IceCube-Gen2 [22]. The design choices of the radio part of IceCube-Gen2 are strongly influenced by the performance of the RNO-G components.

References

[1] RNO-G collaboration *JINST* **16** no. 03, (2021) P03025. [Err: JINST 18, E03001 (2023)].
[2] S. Barwick and C. Glaser *arXiv* **2208.04971** (2022) .
[3] J. Rix *et al. Journal of Glaciology* **65** no. 250, (2019) 288–298.
[4] B. Hendricks for the RNO-G collaboration, *PoS* **ICRC2023** (2023) 1133.
[5] B. Oeyen for the RNO-G collaboration, *PoS* **ICRC2023** (2023) 1042.
[6] C. Welling for the RNO-G collaboration, *PoS* **ICRC2023** (2023) 1054.
[7] E. Oberla for the RNO-G collaboration, *PoS* **ICRC2023** (2023) 1171.
[8] RNO-G collaboration, *PoS* **ARENA2022** (2023) 005.
[9] J. A. Aguilar *et al. Astropart. Phys.* **145** (2023) 102790.
[10] T. Glüsenkamp for the RNO-G collaboration, *PoS* **ICRC2023** (2023) 1056.
[11] Z. Meyers for the RNO-G collaboration, *PoS* **ICRC2023** (2023) 1142.
[12] C. Glaser *et al. Eur. Phys. J. C* **79** no. 6, (2019) 464.
[13] M. Büsken, T. Fodran, and T. Huege *arXiv* **2211.03086** (2022) .
[14] C. Marque *et al.*, 2008. https://doi.org/10.24414/nrdh-c565.
[15] We acknowledge the Fachhochschule Nordwestschweiz (FHNW) Campus Brugg/Windisch and Instituto Ricerche Solari (IRSOL) Locarno, Switzerland for providing the CALLISTO data. C. Monstein, A. Csillaghy, and A. O. Benz, "CALLISTO Solar Spectrogram FITS files [Data set], International Space Weather Initiative (ISWI)," 2023. https://doi.org/10.48322/pmwd-mk15.
[16] L. Pyras and I. Plaisier for the RNO-G collaboration, *PoS* **ECRS2022** (2022) 088.
[17] J. Henrichs for the RNO-G collaboration, *PoS* **ICRC2023** (2023) 259.
[18] L. Pyras et al., *PoS* **ICRC2023** (2023) 1076.
[19] I. Plaisier, S. Bouma, and A. Nelles *Eur. Phys. J. C* **83** no. 5, (2023) 443.
[20] M. Muzio for the RNO-G collaboration, *PoS* **ICRC2023** (2023) 1485.
[21] A. Coleman for the RNO-G collaboration, *PoS* **ICRC2023** (2023) 1100.
[22] IceCube collaboration, 2023. https://icecube-gen2.wisc.edu/science/publications/TDR.

Full Author List: RNO-G Collaboration

J. A. Aguilar[1], P. Allison[2], D. Besson[3], A. Bishop[10], O. Botner[4], S. Bouma[5], S. Buitink[6], W. Castiglioni[8], M. Cataldo[5], B. A. Clark[7], A. Coleman[4], K. Couberly[3], P. Dasgupta[1], S. de Kockere[9], K. D. de Vries[9], C. Deaconu[8], M. A. DuVernois[10], A. Eimer[5], C. Glaser[4], T. Glüsenkamp[4], A. Hallgren[4], S. Hallmann[11], J. C. Hanson[12], B. Hendricks[14], J. Henrichs[11,5], N. Heyer[4], C. Hornhuber[3], K. Hughes[8], T. Karg[11], A. Karle[10], J. L. Kelley[10], M. Korntheuer[1], M. Kowalski[11,15], I. Kravchenko[16], R. Krebs[14], R. Lahmann[5], P. Lehmann[5], U. Latif[9], P. Laub[5], C.-H. Liu[16], J. Mammo[16], M. J. Marsee[17], Z. S. Meyers[11,5], M. Mikhailova[3], K. Michaels[8], K. Mulrey[13], M. Muzio[14], A. Nelles[11,5], A. Novikov[19], A. Nozdrina[3], E. Oberla[8], B. Oeyen[18], I. Plaisier[5,11], N. Punsuebsay[19], L. Pyras[11,5], D. Ryckbosch[18], F. Schlüter[1], O. Scholten[9,20], D. Seckel[19], M. F. H. Seikh[3], D. Smith[8], J. Stoffels[9], D. Southall[8], K. Terveer[5], S. Toscano[1], D. Tosi[10], D. J. Van Den Broeck[9,6], N. van Eijndhoven[9], A. G. Vieregg[8], J. Z. Vischer[5], C. Welling[8], D. R. Williams[17], S. Wissel[14], R. Young[3], A. Zink[5]

[1] Université Libre de Bruxelles, Science Faculty CP230, B-1050 Brussels, Belgium
[2] Dept. of Physics, Center for Cosmology and AstroParticle Physics, Ohio State University, Columbus, OH 43210, USA
[3] University of Kansas, Dept. of Physics and Astronomy, Lawrence, KS 66045, USA
[4] Uppsala University, Dept. of Physics and Astronomy, Uppsala, SE-752 37, Sweden
[5] Erlangen Center for Astroparticle Physics (ECAP), Friedrich-Alexander-University Erlangen-Nürnberg, 91058 Erlangen, Germany
[6] Vrije Universiteit Brussel, Astrophysical Institute, Pleinlaan 2, 1050 Brussels, Belgium
[7] Department of Physics, University of Maryland, College Park, MD 20742, USA
[8] Dept. of Physics, Enrico Fermi Inst., Kavli Inst. for Cosmological Physics, University of Chicago, Chicago, IL 60637, USA
[9] Vrije Universiteit Brussel, Dienst ELEM, B-1050 Brussels, Belgium
[10] Wisconsin IceCube Particle Astrophysics Center (WIPAC) and Dept. of Physics, University of Wisconsin-Madison, Madison, WI 53703, USA
[11] Deutsches Elektronen-Synchrotron DESY, Platanenallee 6, 15738 Zeuthen, Germany
[12] Whittier College, Whittier, CA 90602, USA
[13] Dept. of Astrophysics/IMAPP, Radboud University, PO Box 9010, 6500 GL, The Netherlands
[14] Dept. of Physics, Dept. of Astronomy & Astrophysics, Penn State University, University Park, PA 16801, USA
[15] Institut für Physik, Humboldt-Universität zu Berlin, 12489 Berlin, Germany
[16] Dept. of Physics and Astronomy, Univ. of Nebraska-Lincoln, NE, 68588, USA
[17] Dept. of Physics and Astronomy, University of Alabama, Tuscaloosa, AL 35487, USA
[18] Ghent University, Dept. of Physics and Astronomy, B-9000 Gent, Belgium
[19] Dept. of Physics and Astronomy, University of Delaware, Newark, DE 19716, USA
[20] Kapteyn Institute, University of Groningen, Groningen, The Netherlands

Acknowledgments

We are thankful to the staff at Summit Station for supporting our deployment work in every way possible. We also acknowledge our colleagues from the British Antarctic Survey for embarking on the journey of building and operating the BigRAID drill for our project. We would like to acknowledge our home institutions and funding agencies for supporting the RNO-G work; in particular the Belgian Funds for Scientific Research (FRS-FNRS and FWO) and the FWO programme for International Research Infrastructure (IRI), the National Science Foundation (NSF Award IDs 2118315, 2112352, 211232, 2111410) and the IceCube EPSCoR Initiative (Award ID 2019597), the German research foundation (DFG, Grant NE 2031/2-1), the Helmholtz Association (Initiative and Networking Fund, W2/W3 Program), the University of Chicago Research Computing Center, and the European Research Council under the European Unions Horizon 2020 research and innovation programme (grant agreement No 805486).